

1 **Comprehensive Quantification of Height Dependence of**
2 **Entrainment-Mixing between Stratiform Cloud Top and**
3 **Environment**

4 Sinan Gao¹, Chunsong Lu^{1*}, Yangang Liu², Seong Soo Yum³, Jiashan Zhu¹, Lei Zhu¹, Neel Desai^{2a},
5 Yongfeng Ma⁴, Shang Wu¹

6 ¹Collaborative Innovation Center on Forecast and Evaluation of Meteorological Disasters, Key Laboratory for Aerosol-
7 Cloud-Precipitation of China Meteorological Administration, Nanjing University of Information Science & Technology,
8 Nanjing, China

9 ²Environmental and Climate Sciences Department, Brookhaven National Laboratory, Upton NY, US

10 ³Department of Atmospheric Sciences, Yonsei University, Seoul, South Korea

11 ⁴Department of Mechanics & Aerospace Engineering, Southern University of Science and Technology, Shenzhen, China

12 *Correspondence to:* Chunsong Lu (luchunsong110@gmail.com)

13

^a Now at Department of Meteorology and Climate Science, San Jose State University, San Jose, CA

14 **Abstract.** Different entrainment-mixing processes of turbulence are crucial to processes related to clouds; however, only a
15 few qualitative studies have been concentrated on the vertical distributions of entrainment-mixing mechanisms with low
16 vertical resolutions. To quantitatively study vertical profiles of entrainment-mixing mechanisms with a high resolution, the
17 stratiform clouds observed in the Physics of Stratocumulus Top (POST) project are examined. The unique sawtooth flight
18 pattern allows for an examination of the vertical distributions of entrainment-mixing mechanisms with a 5 m vertical
19 resolution. Relative standard deviation of volume mean radius divided by relative standard deviation of liquid water content
20 is introduced to be a new estimation of microphysical homogeneous mixing degree, to overcome difficulties of determining
21 the adiabatic microphysical properties required in existing measures. The vertical profile of this new measure indicates that
22 entrainment-mixing mechanisms become more homogeneous with decreasing altitudes and are consistent with the dynamical
23 measures of Damkohler number and transition scale number. Further analysis shows that the vertical variation of
24 entrainment-mixing mechanisms with decreasing altitudes is due to the increases of turbulent dissipation rate in cloud and
25 relative humidity in droplet-free air, and the decrease of size of droplet-free air. The results offer insights into the theoretical
26 understanding and parameterizations of vertical variation of entrainment-mixing mechanisms.

27

28 **1 Introduction**

29 Clouds are identified to be a significant origin of uncertainties in climate research, because of poor simulations of clouds
30 (Bony and Dufresne, 2005; Stephens, 2005; Zheng and Rosenfeld, 2015; Zhao and Garrett, 2015; Wang et al., 2019; Cess et
31 al., 1989; Wang, 2015; Gao et al., 2016; Grabowski, 2006; Morrison, 2015). Entrainment-mixing processes of turbulence
32 have been considered as significant factors for various processes related to clouds (Su et al., 1998; Lasher - trapp et al., 2005;
33 Hoffmann and Feingold, 2019; Xu et al., 2020; Hudson et al., 1997; Liu et al., 2002). Therefore, it is vital to figure out the
34 nature of interaction between clouds and environment and their impacts on cloud droplet properties (Xue and Feingold,
35 2006). Entrainment-mixing processes are considered to occur primarily near the stratiform cloud top and entrainment-mixing
36 around the stratiform cloud sides is negligible (Wood, 2012; Xu and Xue, 2015).

37

38 The question about how entrained air affects cloud microphysics has been debated for a long time. Several conceptual
39 models have been established to study the different entrainment-mixing processes, e.g., entity-type entrainment-mixing
40 (Telford, 1996; Telford and Chai, 1980), vertical circulation entrainment-mixing (Yeom et al., 2017; Yum et al., 2015; Wang
41 et al., 2009) and homogeneous (HM)/inhomogeneous (IM) entrainment-mixing (Baker et al., 1980; Baker et al., 1984). The
42 last one is the most used and studied. During the HM mixing, the time scale for droplets to evaporate completely is larger
43 than the time scale for mixing between entrained air and cloudy air. All droplets are exposed to the same unsaturated state
44 and evaporate concurrently. In this scenario, all droplets' sizes decrease simultaneously, and number concentration also
45 decreases due to the dilution effect of entrained air. While in the IM mixing, mixing time scale is larger than evaporation
46 time scale. Some droplets adjacent to entrained air would evaporate completely to saturate the air, while the other droplets
47 are not affected by the entrainment. In this scenario, number concentration decreases but droplet size remains unchanged.
48 Some observational studies support the extreme IM concept (Burnet and Brenguier, 2007; Lu et al., 2011; Freud et al., 2011;
49 Pawlowska et al., 2000; Haman et al., 2007; Freud et al., 2008); while some others indicate that the HM mixing dominates
50 (Gerber et al., 2008; Lu et al., 2013c; Burnet and Brenguier, 2007; Jensen et al., 1985), and still some others find
51 intermediate features fall in between the HM and IM mixing (Lehmann et al., 2009; Lu et al., 2014a; Kumar et al., 2018).

52

53 The vertical variation of entrainment-mixing mechanisms is less studied. For cumulus, Small et al. (2013) and Jarecka et al.
54 (2013) found that a trend existed of entrainment-mixing to be more HM in cloud top, resulted from increasing of cloud
55 droplet radius and turbulence with increasing altitudes. In stratiform clouds, Yum et al. (2015) and Wang et al. (2009)
56 observed positive correlation at middle of cloud and no correlation at cloud top between droplet size and liquid water content.
57 Yum et al. (2015) suggested that entrainment mixing at cloud top region was indeed IM, while during the descent of vertical
58 circulation, the cloud droplets in more diluted parcels would evaporate faster, and observe the generally HM feature at a

59 relatively long depth from cloud top.

60

61 The above few studies are largely qualitative and based on horizontal flight legs with coarse vertical resolutions.
62 Furthermore, these studies often need to determine adiabatic cloud microphysical properties from observational data, which
63 are full of known and unknown uncertainties (e.g., Jensen et al., 1985; Yum et al., 2015; Lu et al., 2014b; Yeom et al., 2017).

64

65 This study aims to overcome these limitations by examining the data from the field campaign of Physics of Stratocumulus
66 Top (POST) (Hill et al., 2010; Malinowski et al., 2010; Gerber et al., 2010) for the high-resolution vertical variation of
67 entrainment-mixing processes. Four measures of microphysical homogeneous mixing degrees (HMDs) that require the
68 determination of adiabatic cloud properties (Lu et al., 2014b; Lu et al., 2013b; Lu et al., 2014a) are examined and
69 inconsistencies are discussed. A new microphysical measure is proposed to quantify the entrainment-mixing mechanisms to
70 overcome the drawbacks of the existing methods that require cloud adiabatic properties. Physical reasons for the vertical
71 variation of entrainment-mixing mechanisms are analyzed using a comprehensive microphysical-dynamical approach.

72

73 The rest of this study is presented as follows. The POST dataset and the existing methods for calculating microphysical and
74 dynamical measures of HMD are presented in Section 2. Section 3 first shows the analysis of entrainment-mixing
75 mechanisms using the existing microphysical measures and dynamical measures. A new microphysical measure is then
76 introduced to represent entrainment-mixing mechanisms after discussing the potential uncertainties in choosing and
77 determining the adiabatic properties needed for the existing microphysical measures. The key factors affecting vertical
78 variation of entrainment-mixing are examined as well. Section 4 is the concluding remarks.

79 **2 Dataset and Methods**

80 **2.1 Dataset**

81 POST was designed to further the understanding of the physical processes around stratiform cloud top zone (Carman et al.,
82 2012; Gerber et al., 2010; Hill et al., 2010; Malinowski et al., 2010; Ma et al., 2017; Jen-La Plante et al., 2016; Ma et al.,
83 2018; Kumala et al., 2013). During POST campaign, thermodynamic, dynamical, and microphysical properties were
84 measured on board in July and August of 2008 with a total of 17 research flights. Flights were implemented in the vicinity of
85 the coast of Santa Cruz/Monterey, California, US, within 36° to 37° N and 123° to 124° W (Gerber et al., 2010; Hill et al., 2010;
86 Malinowski et al., 2010).

87

88 **The Cloud and Aerosol Spectrometer (CAS) probe measured size distributions in the radius range of 0.29 - 25.5 μ m at the**

89 frequency of 10 Hz. The data in the radius range of 1.0 - 25.5 μm are used to calculate microphysical properties, i.e., number
90 concentration (n_c), liquid water content (LWC_c) and volume mean radius (r_{vc}). The Modified Ultrafast Thermometer (UFT-M)
91 was the temperature probe. Only the flights with good quality temperature data (no reports of “noise”, “spike” or “holes in
92 the data” in the data description file) are used. Although the time resolution of temperature data was as high as 1000 Hz
93 (Kumala et al., 2013), 10 Hz data are used here. Humidity was measured by the EDGETECH EG&G Chilled Mirror at 10
94 Hz. For turbulence measurements, the five-hole gust detector provided by University of California, Irvine (UCI) was used to
95 collect high resolution wind velocities at 40 Hz. We use 10 cm^{-3} of n_c and 0.001 g m^{-3} of LWC_c to be the standard of
96 threshold values to select cloudy samples (Lu et al., 2014b; Deng et al., 2009; Zhang et al., 2011). We define the cloud base
97 as the lowest altitudes where the samples satisfy the previously mentioned cloud criteria. We focus only on the non-drizzling
98 clouds, and the threshold value of drizzle water content in cloud using Cloud Imaging Probe (CIP) measurements (radius
99 larger than 25 μm) is 0.005 g m^{-3} (Lu et al., 2011). A total of 4 flights in POST (July 16, August 02, 06, 08, 2008) satisfying
100 the above criteria is selected to examine the vertical variation of entrainment-mixing mechanisms.

101 2.2 Sawtooth Pattern Flights

102 Unlike most aircraft campaigns, the POST flights were designed as sawtooth legs to examine detailly the vertical structures
103 of the stratiform cloud top zone (Figure 1 (a)) (Carman et al., 2012; Gerber et al., 2013; Jen-La Plante et al., 2016). About 60
104 sawtooth legs are contained in each flight (Gerber et al., 2013; Carman et al., 2012). In this way, high-resolution vertical
105 profiles near cloud top can be obtained, which are not available from the conventional sampling along horizontal legs.
106 Because the cloud top altitudes vary spatially, we calculate the average cloud top altitude measured by each sawtooth profile
107 and only the sawtooth legs with cloud tops 30 m above/below the average cloud top are selected. The procedure of altitude
108 stratification is illustrated in Figure 1 (b). We take 5 m as the vertical interval of all sawtooth patterns. All the analyses below
109 are based on the cloud properties averaged over the 5 m vertical intervals and each vertical interval consists of thousands of
110 data. Only the height intervals over which the average droplet-free air sizes (i.e., non-cloudy sample sizes between cloudy
111 samples) are larger than zero are analyzed, which is detailed later in Figure 10. The results are similar when the vertical
112 resolution of all sawtooth patterns is set as 3 m and 7 m, respectively (not shown).

113 2.3 Methods

114 2.3.1 Existing Microphysical Measures of Homogeneous Mixing Degree

115 Based on the diagram of microphysical mixing, four HMDs have been defined to contain all kinds of entrainment mixing
116 mechanisms. The first three measures are based on the diagram of r_{vc}^3/r_{va}^3 versus n_c/n_a (Lu et al., 2014a; Lu et al., 2013b), as

117 shown in Figure 2 (a) and (b). Figure 2 (a) declares the various status during a whole process of entrainment-mixing for
 118 defining the first measure (ψ_1). The adiabatic cloud is represented by Point A with the number concentration (n_a) and volume
 119 mean radius (r_{va}) of adiabatic state. After environmental air is entrained into cloud, the state of cloud approaches Point B,
 120 which number concentration is n_h and volume mean radius is r_{va} . Then mixing and evaporation processes occur and cloud
 121 state approaches Point C, where number concentration after evaporation is n_c and volume mean radius after evaporation is r_{vc} .
 122 The included angle between the line connecting Point B to Point E and the extreme IM mixing line is $\pi/2$, and the included
 123 angle between the line connecting Point B to Point C and the extreme IM mixing line is β . Then ψ_1 is defined as:

$$124 \quad \psi_1 = \frac{\beta}{\pi/2}, \quad (1a)$$

125 where β is

$$126 \quad \beta = \arctan\left(\frac{r_{vc}^3/r_{va}^3 - 1}{n_c/n_a - n_h/n_a}\right); \quad (1b)$$

127 $n_h = n_a \times \chi$ and χ represents the adiabatic cloud fraction after mixing derived from energy conservation and total water
 128 conservation in the isobaric mixing (Lehmann et al., 2009; Gerber et al., 2008; Lu et al., 2012). The second HMD (ψ_2) is
 129 defined in view of Figure 1 (b):

$$130 \quad \psi_2 = \frac{1}{2} \left(\frac{n_c - n_i}{n_h - n_i} + \frac{r_{vc}^3 - r_{va}^3}{r_{vh}^3 - r_{va}^3} \right), \quad (2)$$

$$131 \quad \text{where } n_i = \frac{r_{vc}^3}{r_{va}^3} n_c \text{ and} \quad (3)$$

$$132 \quad r_{vh}^3 = \frac{n_c}{n_h} r_{vc}^3. \quad (4)$$

133 Here n_i is the number concentration after extreme IM mixing and r_{vh} is the volume mean radius after HM mixing. The third
 134 measure of HMD (ψ_3) is given by

$$135 \quad \psi_3 = \frac{\ln(n_c) - \ln(n_i)}{\ln(n_h) - \ln(n_i)} = \frac{\ln(r_{vc}^3) - \ln(r_{va}^3)}{\ln(r_{vh}^3) - \ln(r_{va}^3)}. \quad (5)$$

136 The fourth measure (ψ_4) is defined using mixing diagram of r_{vc}^3/r_{va}^3 versus LWC_c/LWC_a (Lu et al., 2014b), as shown in
 137 Figure 2 (c),

$$138 \quad \psi_4 = \frac{1 - r_{vc}^3/r_{va}^3}{1 - LWC_c/(\chi LWC_a)}. \quad (6)$$

139 The meanings of the Points A - E are the same as those in Figures 2 (a) and 2 (b). Four kinds of HMDs are expected to range

140 from 0 to 1, the higher probability of HM mixing corresponds to the larger HMD value.

141

142 A new dimensionless HMD (ψ_5) is introduced to quantify the different entrainment-mixing mechanisms:

$$143 \psi_5 = \text{dis}(r_{vc}^3) / \text{dis}(\text{LWC}_c), \quad (7)$$

144 where *dis* represents the relative standard deviation expressed by the ratio of standard deviation to the average value over
145 each level. During entrainment-mixing and evaporation processes, LWC_c always decreases but r_{vc} decreases in the HM
146 mixing and remains constant in the extreme IM mixing. Therefore, the extreme IM mixing corresponds to $\psi_5 = 0$, and the
147 larger the value of ψ_5 is, the more HM the entrainment mixing is. More discussions on ψ_5 are given in Section 3.2.

148 2.3.2 Dynamical Measures of Homogeneous Mixing Degree

149 The dynamical aspect, i.e., the mixing process between cloud and environment air vs. the evaporation process of cloud
150 droplets, is important to distinguish different entrainment-mixing mechanisms (Baker et al., 1980; Baker and Latham, 1979).
151 The mixing time scale divided by evaporation time scale is defined as Damkohler number (Da), which is usually used to
152 quantify mixing process is faster or evaporation process is faster and thus to discern the entrainment-mixing mechanisms
153 (Siebert et al., 2006; Burnet and Brenguier, 2007; Andrejczuk et al., 2009),

$$154 Da = \frac{\tau_{\text{mix}}}{\tau_r}, \quad (8)$$

155 where τ_{mix} and τ_r are turbulent mixing time and microphysical response time of droplets, respectively (Lehmann et al., 2009).
156 A more IM mixing corresponds to a larger Da . Three kinds of microphysical time scales, phase relaxation time (τ_{phase})
157 (Kumar et al., 2013; Kumar et al., 2012), evaporation time (τ_{evap}) (Andrejczuk et al., 2009; Baker et al., 1980; Burnet and
158 Brenguier, 2007), and reaction time (τ_{react}) (Lehmann et al., 2009; Lu et al., 2011; Lu et al., 2013c; Lu et al., 2014b), have
159 been used to represent τ_r . Lu et al. (2018) found that the most appropriate time scale was τ_{evap} if we focus on the changes of
160 number concentration and radius of droplets. The mixing time scale is defined as follows:

$$161 \tau_{\text{mix}} \sim (L^3 / \varepsilon)^{1/3}, \quad (9)$$

162 where ε is the turbulent dissipation rate calculated from the three dimensional wind velocities (Meischner et al., 2001) (see
163 Appendix A for details), and L is the size of droplet-free air calculated with

$$164 L = F \times \text{TAS} / f, \quad (10)$$

165 where droplet-free sample size divided by the sum of cloud and droplet-free sample size is considered as fraction of droplet-
166 free F in each vertical interval (e.g., if there are 90 cloud samples and 10 non-cloudy samples, $F = 10/(10+90) = 10\%$); TAS

167 and f are the aircraft true air speed ($\sim 55 \text{ m s}^{-1}$) and sampling frequency (10 Hz), respectively. The size of droplet-free air is
 168 used as a proxy for the entrained air parcels' size. In equation (8), the time scale for a droplet of radius r_{va} to completely
 169 evaporate (evaporate time) is given by:

$$170 \quad \tau_{\text{evap}} = -\frac{r_{va}^2}{2AS_0}, \quad (11)$$

171 where S_0 is the supersaturation of the droplet-free air at the corresponding altitude (Yau and Rogers, 1996); A is affected by
 172 air temperature and pressure (see Appendix B for details).

173

174 Another dynamical measure given by the ratio of L^* to η is transition scale number (N_L) (Lu et al. (2011)):

$$175 \quad N_L = \frac{L^*}{\eta}, \quad (12)$$

176 where transition length (L^*) is considered as the corresponding L value when $Da = 1$ (Lehmann et al., 2009) and is given as
 177 follows:

$$178 \quad L^* = \varepsilon^{1/2} \tau_r^{3/2}. \quad (13)$$

179 In equation (12), η is the Kolmogorov length scale (Wyngaard, 2010), which is given by:

$$180 \quad \eta = \left(\frac{\nu^3}{\varepsilon}\right)^{1/4}, \quad (14)$$

181 where ν is the kinematic viscosity (Wyngaard, 2010). A higher probability of HM mixing corresponds to a larger value of N_L .

182 **3 Results**

183 **3.1 Entrainment-Mixing Mechanisms from the Microphysical and Dynamical Perspectives**

184 It has been known that it can be uncertain and even problematic to determine the representative adiabatic values from the
 185 observational data needed in calculation of the above-mentioned microphysical measures (Yeom et al., 2017; Jensen et al.,
 186 1985; Yum et al., 2015). For example, because vertical velocity and concentration of cloud condensation nuclei can change
 187 spatially in clouds, n_a and r_{va} change accordingly. Entrainment-mixing in clouds adds difficulties to determine accurate
 188 values of r_{va} , n_a and LWC_a . Improper estimation of adiabatic values may violate the theoretical expectation: $n_a \geq n_h \geq n_c \geq n_i$
 189 and $r_{va} \geq r_v$, and then cause unrealistic HMDs. Different adiabatic variables have been used in previous studies. For example,
 190 the maximum volume mean radius and number concentration are used as proxy values for r_{va} and n_a for each horizontal
 191 penetration, respectively (Yeom et al., 2017; Yum et al., 2015); LWC_a is calculated from the adiabatic growth from cloud

192 base, and the maximum number concentration of whole flight penetration is considered as n_a (Burnet and Brenguier, 2007;
193 Lehmann et al., 2009); n_a is the mean value of top 2% of n_c for each flight and r_{va} is calculated using adiabatic water vapor
194 mixing ratio, adiabatic total water mixing ratio and n_a for a horizontal penetration (Small et al., 2013).

195

196 To examine the influence of using different adiabatic properties, we compare ψ_i ($i = 1 - 4$) calculated with different adiabatic
197 variables (Table 1) at each level near the stratiform cloud tops for the data collected during the four flights. Only the results
198 for the first microphysical measure are shown in Figure 3; the other results are shown in the Supporting Information. In
199 Figure 3, LWC_a is based on the adiabatic growth from cloud base, the maximum number concentration at each level is
200 assumed as n_a , and r_{va} is calculated from LWC_a and n_a . In Figure S1, LWC_a is based on the adiabatic growth from cloud base,
201 the maximum volume mean radius at each level is assumed as r_{va} , and n_a is calculated from LWC_a and r_{va} . In Figure S2, the
202 maximum liquid water content at each level is assumed as LWC_a , the maximum number concentration at each level is
203 assumed as n_a , and r_{va} is calculated from LWC_a and n_a . In Figure S3, the maximum liquid water content at each level is
204 assumed as LWC_a , the maximum volume mean radius at each level is assumed as r_{va} , and n_a is calculated from LWC_a and r_{va} .
205 In Figure S4, the maximum number concentration at each level is assumed as n_a , the maximum volume mean radius at each
206 level is assumed as r_{va} , and LWC_a is calculated from n_a and r_{va} . According to the definitions, ψ_i ($i = 1 - 4$) are expected to
207 range from 0 to 1. However, some values of ψ_i ($i = 1 - 4$) are larger than 1 or smaller than 0 in Figure 3 and Figures S1 – S4,
208 which could be caused by uncertainties in r_{va} , LWC_a , n_a and cloud base (Lu et al., 2014b; Lu et al., 2014a; Lu et al., 2013b;
209 Gerber et al., 2008). Furthermore, these figures suggest different vertical distributions of HMDs for the same flight,
210 suggesting that high sensitivity of the conventional HMDs to the methods for determining the adiabatic values could pose a
211 serious problem as to which figure represents the reality of entrainment-mixing mechanisms.

212

213 Since the above analysis from the microphysical perspective does not tell a consistent story about the vertical variation of
214 HMD, Da and N_L are examined from the dynamical perspective. Figures 4 (a), (c), (e) and (g) show the height dependence of
215 Da during each of the four flights. It is obvious that Da decreases with decreasing altitudes. Figures 4 (b), (d), (f) and (h)
216 show a significant increasing trend of N_L with decreasing altitudes. The method for setting the adiabatic values in Figure 4 is
217 the same as that in Figure 3, i.e., LWC_a is based on the adiabatic growth from cloud base, the maximum number
218 concentration at each level is assumed as n_a , and r_{va} is calculated from LWC_a and n_a . Unlike the microphysical measures,
219 vertical variation of Da or N_L are similar when different methods for determining adiabatic values are used (Figures S5 – S8).
220 It is expected that a smaller Da (larger N_L) represents a larger HMD. The results of Da and N_L both suggest more IM mixing
221 closer to cloud top. It is noteworthy that this result is robust, not affected by the methods for obtaining the adiabatic values,
222 and thus should reflect the real height dependence of entrainment-mixing mechanisms.

223

224 The different vertical distributions of HMDs and the inconsistency between microphysical HMDs and dynamical measures
 225 are mainly due to the improper estimations of adiabatic values. For example, during the flight of 16 July in Figure 3, the
 226 HMDs decrease with the decreasing altitudes, and most of the HMDs are negative. The negative values do not meet the
 227 theoretical expectations and these trends are completely inconsistent with those of dynamical measures. The vertical
 228 variations of some important properties of this case are shown in Figure 5. The negative values of HMDs are due to
 229 unexpected result of $r_{va} \leq r_{vc}$. Under these circumstances, the difference between r_{vc} and r_{va} becomes larger with the
 230 decreasing altitudes, corresponding to the decreasing trends of HMDs with the decreasing altitudes. Besides the first method,
 231 the other four methods mentioned above also have their own unreasonable points. For example, $r_{va} \leq r_{vc}$ exists under the
 232 methods 1, 3 and 4; $n_a \leq n_c$ exists under the methods 2 and 4; r_{va} does not always increase with the increasing altitudes under
 233 the methods 2, 4 and 5 (See figures S9 to S13 for details). Overall, the inconsistency among the microphysical HMDs
 234 estimated with different methods to determine the adiabatic variables calls for a new microphysical measure of entrainment-
 235 mixing mechanisms.

236 3.2 New Microphysical Measure

237 As discussed in Section 3.1, the existing microphysical measures of HMDs depend on the different adiabatic values to a
 238 great extent. In order to avoid this kind of uncertainty, a new dimensionless HMD (ψ_5) in equation (7) is introduced to
 239 quantify the different entrainment-mixing mechanisms. To make sure that ψ_5 is applied properly, the correlation between r_{vc}^3
 240 and LWC_c must be positive. If the correlation is negative, IM mixing with subsequent ascent is likely to occur (Lu et al.,
 241 2013a; Lehmann et al., 2009; Wang et al., 2009; Siebert et al., 2006; Lasher - trapp et al., 2005). It is worth mentioning that
 242 ψ_5 does not require using adiabatic values, and thus can overcome the deficiencies of ψ_i ($i = 1 - 4$) associated with choosing
 243 different adiabatic cloud properties.

244
 245 The vertical variation of ψ_5 for the 4 flights are shown in Figure 6. The small value of ψ_5 near the cloud tops shows that
 246 entrainment-mixing approaches extreme IM, consistent with conclusions in several previous studies based on the POST data
 247 (Gerber et al., 2013; Gerber et al., 2016; Malinowski et al., 2013). The increase of ψ_5 with decreasing altitudes indicates that
 248 the trends towards more HM with the decreasing altitudes, consistent with the results of Da and N_L (Figure 4 and Figures S5
 249 – S8). We also check the relationship between r_{vc}^3 and LWC_c and the two quantities are positively correlated (not shown).

250
 251 The relationships between ψ_5 versus Da and N_L of the 4 flights are shown in Figure 7 and are well fitted by the equations
 252 used in Luo et al. (2020)

$$253 \quad \psi_5 = a_1 \exp(b_1 Da^{c_1}), \quad (15)$$

$$\psi_5 = a_2 \exp(b_2 N_L^{c_2}), \quad (16)$$

where the parameters a_1 and a_2 are positive; b_1 and b_2 are negative; c_1 is positive and c_2 is negative. The negative correlation of ψ_5 vs Da and positive correlation of ψ_5 vs N_L are evident and in keeping with theoretical arguments, suggesting that a smaller Da or a larger N_L corresponds to a higher ψ_5 . Such relationships further confirm the utility and applicability of ψ_5 in studying entrainment-mixing mechanisms. The correlation coefficients of the linear regression of for ψ_5 vs Da and ψ_5 vs N_L are about 0.66 and 0.60, respectively, suggesting that Da and N_L are basically equivalent for understanding the entrainment-mixing parameterization.

The equivalence of Da and N_L is further supported by the tight negative correlation between Da and N_L (Figure 8). Similar results have been reported in Gao et al. (2018) using numerical simulations, and Desai et al. (2021) based on holographic measurements. However, the underlying reasons are different. Figure 9 shows that L and L^* are negatively correlated, opposite to the positive correlation between L^* and the Taylor microscale in Gao et al. (2018); Taylor microscale is used as L in the calculation of τ_{mix} in equation (9) in Gao et al. (2018). It is easy to derive from equations (8), (9), (11) and (12) that $Da : N_L = L : L^*$, others being equal:

$$\frac{Da}{N_L} = \frac{-2AS_0\eta}{\varepsilon^{1/3}r_{\text{va}}^2} \cdot \frac{L}{L^*} \quad (17)$$

Therefore, as long as L and L^* are nearly linearly correlated, Da and N_L are equivalent. When extreme IM mixing dominates near cloud top, ε is small (Figure 10), which mainly determines small L^* ; L is large near cloud top (Figure 10). Therefore, L and L^* are negatively correlated. The vertical distributions of affecting factors on entrainment-mixing are detailed in the next sub-section.

3.3 Further analysis of Affecting Factors

According to the analyses in Sections 3.1 and 3.2, the dynamical and microphysical measures both indicate that entrainment-mixing mechanisms change from IM to HM with decreasing altitudes. Here we provide the physical explanation for such behavior under the framework of HM/IM entrainment-mixing mechanisms, by analyzing the vertical variations of all the variables defining Da and N_L , i.e., ε , relative humidity (RH) and L .

First, Figures 10 (a), (d), (g) and (j) show that ε increases with decreasing altitudes, which is opposite to that for cumulus clouds (Small et al. (2013) and Jarecka et al. (2013)). According to definition of Da (equation (8)) and N_L (equation (12)), the increase of ε leads to the decrease of Da and increase of N_L , others being equal. Therefore, ε is an important factor to

283 cause Da to decrease and N_L to increase with the decreasing altitudes (Figure 4 and Figures S5 – S8). The clouds were
284 sampled in the vicinity of the coast of Santa Cruz/Monterey, California, therefore, these clouds were well-mixed and coupled,
285 which explains the monotonic decrease of ε with the increasing height (Jones et al., 2011; Shupe et al., 2013). Note that
286 the decoupled clouds should be very common in the downstream regions (Bretherton and Wyant, 1997) and midlatitudes
287 (Zheng et al., 2020). The boundary layer decoupling causes a decrease of turbulent kinetic energy near the cloud base,
288 leading to a local minimum near the cloud base and a maximum in the middle of cloud layer which can be used to infer the
289 profile of ε (Stevens, 2000). This is also demonstrated in the observations by Zheng et al. (2016) who found a significant role
290 of decoupling in weakening the cloud-base updrafts. Therefore, in the future studies of decoupled stratocumulus in other
291 regions, the results about entrainment-mixing mechanisms could be different due to the non-monotonic vertical variation of ε .

292
293 Second, the vertical variation of entrainment-mixing can also be attributed to that of entrained air sizes. Figures 10 (b), (e),
294 (h) and (k) show that L decreases significantly with decreasing altitudes, which leads to a decrease of Da with decreasing
295 altitudes since Da is proportional to τ_{mix} , and thus L . The importance of L has rarely been studied in previous literatures for
296 height dependence of entrainment-mixing. The decrease of L with decreasing altitudes agrees generally with the cascade of
297 breakdown of dry air parcels entrained at the cloud top.

298
299 Third, vertical variation of entrained air RH plays a significant part in determining the entrainment-mixing mechanisms. In
300 former literatures (Yeom et al., 2017; Lu et al., 2018), RH is commonly assumed to be constant across multiple different
301 altitudes when calculating τ_{evap} using $S_0 = \text{RH} - 1$. In fact, RH should not be a constant. We determine RH as the mean RH of
302 droplet-free air in each level. Figures 10 (c), (f), (i) and (l) show that RH increases with decreasing altitudes due to droplet
303 evaporation. According to the definition of Da , Da decreases with the increase of τ_{evap} , and thus decreases with the increase
304 of RH (equation (7) and (10)). Equations (10), (11) and (12) show that N_L increases with increasing RH. Both Da and N_L
305 indicate more HM mixing at a lower altitude. These results suggest that the increases of ε and RH and the decrease of L with
306 decreasing altitudes are in keeping with the variation of entrainment-mixing processes, together playing the primary role in
307 determining the vertical distribution of HMD observed.

308
309 It is noted that, r_{va} also affects Da and N_L through its effect on τ_{evap} . However, r_{va} depends on how adiabatic values are
310 estimated in Section 3.1 (Figure S9 – S14 in the Supporting Information). Therefore, the vertical variation of r_{va} is not
311 analyzed here. No matter which method is used to determine the adiabatic values, the trends of vertical variation of Da and
312 N_L do not change (Section 3.1). The vertical variation of Da and N_L indicates the dominance of the combined effects of ε ,
313 RH and L in determining the vertical variation of entrainment-mixing processes from IM towards HM with decreasing
314 altitudes.

315

316 These results are in keeping with the results drawn in Wang et al. (2009) and Yum et al. (2015) in the sense that a trait of IM
317 mixing is prevalent near cloud top but at mid-levels of clouds a trait of HM mixing becomes dominant, according to the
318 analysis of cloud microphysical relationships at different altitudes of marine stratiform clouds. However, there are big
319 differences in the spatial scale of analysis between our and their studies. We focus on near cloud top regions from cloud top
320 to where droplet-free air patches can still be found, mostly less than 100 m from cloud top (Figure 3). On the other hand,
321 Yum et al. (2015) and Wang et al. (2009) examined mid-levels of stratiform clouds where there remained no droplet-free air
322 patches as well as near cloud top regions. They suggested that the vertical variation of cloud microphysical properties
323 relationships could be caused by vertical circulation of diluted parcels affected by entrainment; the actual mixing near cloud
324 top might have been IM as Da and N_L at this level suggested; as these parcels moved down, the droplets evaporated fast,
325 resulting in cloud microphysical relationships that would be explained as a trait of HM mixing.

326 **4 Concluding Remarks**

327 The observational data of marine stratiform clouds measured from aircraft during the campaign of Physics of Stratocumulus
328 Top (POST) are used to examine the height dependence of entrainment-mixing mechanisms. The sawtooth penetrations are
329 analyzed to acquire fine information on the vertical structure of entrainment-mixing near stratiform cloud tops, from the
330 microphysical and dynamical perspectives. To ensure high vertical resolution, we take 5 m as one altitude distance bin of all
331 sawtooth patterns for the four flights selected in this study.

332

333 From the microphysical perspective, the traditional homogeneous mixing degrees vary distinctly with the decreasing
334 altitudes due to different methods for obtaining adiabatic values. In order to overcome this difficulty, a new homogeneous
335 mixing degree describing the distributions of scatters in the mixing diagram is introduced to quantify different entrainment-
336 mixing mechanisms. The new homogeneous mixing degree is introduced by relative standard deviation of cubic volume
337 mean radius divided by relative standard deviation of liquid water content. If the new homogeneous mixing degree is larger,
338 the mixing is more likely to be homogeneous. The new measure increases with the decreasing altitudes, i.e., more
339 homogeneous with decreasing altitudes. This new measure is not affected by the methods for obtaining adiabatic values and
340 shed new light on the study of entrainment-mixing mechanisms.

341

342 From the dynamical perspective, Damkohler number decreases and transition scale number increases with decreasing
343 altitudes. The relationships between the new homogeneous mixing degree *vs.* Damkohler number and transition scale
344 number are negative and positive, respectively, consistent with theoretical expectation. Therefore, both microphysical and

345 dynamical analyses indicate the trends from inhomogeneous mixing to homogeneous mixing when altitude decreases.

346

347 The factors underlying the vertical variation of entrainment-mixing mechanisms are examined, including vertical
348 distributions of dissipation rate, size of droplet-free air and relative humidity in droplet-free air. Dissipation rate increases
349 and droplet-free air size decreases with the decreasing altitudes. Therefore, mixing is faster at the lower altitude and
350 homogeneous mixing is more likely to occur. Relative humidity increases with decreasing altitudes, which indicates that
351 droplets are less likely to be completely evaporated at the lower altitude. The combined effects of the three factors determine
352 the entrainment-mixing vertical evolution.

353

354 It is noteworthy that the traditional homogeneous mixing degrees are still useful properties to quantify entrainment-mixing
355 mechanisms, if adiabatic values of microphysical properties are properly determined. The new homogeneous mixing degree
356 defined here is a relative measure of homogeneous mixing degree as deviation from the extremely inhomogeneous mixing
357 line, but does not quantify the amount of homogeneous mixing precisely. The relative dispersion of volume-mean radius and
358 liquid water content increases due to differences in mixing states (Khain et al., 2018) and in-cloud activation of cloud
359 condensation nuclei (Derksen et al., 2009; Khain et al., 2018), which affects the calculation of the new homogeneous mixing
360 degree. As pointed out by Khain et al. (2018), the mixing diagram has limitations to analyze entrainment-mixing
361 mechanisms using in situ observations, due to transient mixing states. However, this new measure still provides an
362 alternative method to quantify entrainment-mixing mechanisms, supported by the independent Damkohler and transition
363 scale numbers. This new method can be applied to other datasets with different cloud droplet size probes (e.g., the Forward
364 Scattering Spectrometer Probe, FSSP), since the new definition is based on theoretical understanding of entrainment-mixing
365 mechanisms, which is not limited to the dataset used here. It would be interesting to apply this method to other stratocumulus
366 and cumulus observations in different climate zones.

367

368 **Code and Data Availability**

369 The codes can be accessed by contacting Chunsong Lu via luchunsong110@gmail.com. The POST data is available on
370 <https://archive.eol.ucar.edu/projects/post/>.

371

372 **Author Contributions**

373 SG performed the data analysis and manuscript writing. CL proposed the idea, guided this work and modified the

374 manuscript. YL and SSY supervised this work and helped revise the manuscript. JZ and LZ offered helps to the data
375 analysis. ND, YM and SW also contributed to the modification of manuscript.

376

377 **Competing Interests**

378 The authors declare that they have no conflict of interest.

379

380 **Appendix A**

381 Turbulent dissipation rate (ε) is calculated by three dimensional wind velocities (Meischner et al., 2001)

382
$$\varepsilon \approx \frac{D_{NN}^{3/2}}{(4.01m)^{3/2} d},$$

383 (A1)

384 with $m \approx 0.2(2\pi)^{2/3}$ (Panofsky, 1984). D_{NN} is the local spatial structure function using three wind components and is defined
385 as:

386
$$D_{NN}(t, d) = \frac{1}{3} \left\{ \frac{8}{7} [u(t) - u(t - \frac{d}{TAS})]^2 + \frac{8}{7} [v(t) - v(t - \frac{d}{TAS})]^2 + [w(t) - w(t - \frac{d}{TAS})]^2 \right\},$$
 (A2)

387 where three wind components, east, north and vertical, are represented by u , v and w , respectively; TAS is the aircraft true air
388 speed ($\sim 55m s^{-1}$); t is the time; d is the scale parameter:

389
$$d = TAS \Delta t.$$
 (A3)

390 where Δt is the time interval, which is set to 0.1 s.

391

392 **Appendix B**

393 The parameter A in equation (10) is

394
$$A = \frac{1}{\left[\left(\frac{L_h}{R_v T} - 1\right) \frac{L_h \rho_L}{KT} + \frac{\rho_L R T}{D e_s(T)}\right]}, \quad (\text{B1})$$

395 where R_v , L_h , T , K , ρ_L , D , and $e_s(T)$ are water vapor specific gas constant, latent heat, temperature, coefficient of air thermal
396 conductivity coefficient, liquid water density, water vapor diffusion coefficient in air and vapor pressure of saturation,
397 respectively.

398

399 **Acknowledgment**

400 The authors thank the crew of the POST campaign. This research was supported by the National Key Research and
401 Development Program of China (2019YFA0606803), the Second Tibetan Plateau Scientific Expedition and Research
402 (STEP) program (2019QZKK0105), the National Natural Science Foundation of China (41822504, 42027804, 42075073,
403 41975181), the Innovative Project of Postgraduates in Jiangsu Province in 2020 of Jiangsu (KYCX20_0933) and the China
404 Scholarship Council. Y. Liu is supported by the U. S. Department of Energy Atmospheric System Research (ASR) program
405 (DE-SC00112704) and Solar Energy Technologies Office (SETO) under Award 33504.

406

- 408 Andrejczuk, M., Grabowski, W. W., Malinowski, S. P., and Smolarkiewicz, P. K.: Numerical Simulation of Cloud–Clear Air
 409 Interfacial Mixing: Homogeneous versus Inhomogeneous Mixing, *Journal of the Atmospheric Sciences*, 66, 2493–2500,
 410 10.1175/2009jas2956.1, 2009.
- 411 Baker, M., and Latham, J.: The evolution of droplet spectra and the rate of production of embryonic raindrops in small
 412 cumulus clouds, *Journal of the Atmospheric Sciences*, 36, 1612–1615, 1979.
- 413 Baker, M., Corbin, R., and Latham, J.: The influence of entrainment on the evolution of cloud droplet spectra: I. A model of
 414 inhomogeneous mixing, *Quarterly Journal of the Royal Meteorological Society*, 106, 581–598, 10.1002/qj.49710644914,
 415 1980.
- 416 Baker, M., Breidenthal, R., Choullarton, T., and Latham, J.: The effects of turbulent mixing in clouds, *Journal of the*
 417 *atmospheric sciences*, 41, 299–304, 10.1175/1520-0469(1984)041<0299:TEOTMI>2.0.CO;2, 1984.
- 418 Bony, S., and Dufresne, J. L.: Marine boundary layer clouds at the heart of tropical cloud feedback uncertainties in climate
 419 models, *Geophysical Research Letters*, 32, 10.1029/2005GL023851, 2005.
- 420 Bretherton, C. S., and Wyant, M. C.: Moisture transport, lower-tropospheric stability, and decoupling of cloud-topped
 421 boundary layers, *Journal of Atmospheric Sciences*, 54, 148–167, 1997.
- 422 Burnet, F., and Brenguier, J.-L.: Observational study of the entrainment-mixing process in warm convective clouds, *Journal*
 423 *of the atmospheric sciences*, 64, 1995–2011, 10.1175/JAS3928.1, 2007.
- 424 Carman, J., Rossiter, D., Khelif, D., Jonsson, H., Faloon, I., and Chuang, P.: Observational constraints on entrainment and
 425 the entrainment interface layer in stratocumulus, *Atmospheric Chemistry and Physics*, 12, 11135–11152, 2012.
- 426 Cess, R. D., Potter, G., Blanchet, J., Boer, G., Ghan, S., Kiehl, J., Le Treut, H., Li, Z.-X., Liang, X.-Z., and Mitchell, J.:
 427 Interpretation of cloud-climate feedback as produced by 14 atmospheric general circulation models, *Science*, 245, 513–516,
 428 10.1126/science.245.4917.513 1989.
- 429 Deng, Z., Zhao, C., Zhang, Q., Huang, M., and Ma, X.: Statistical analysis of microphysical properties and the
 430 parameterization of effective radius of warm clouds in Beijing area, *Atmospheric Research*, 93, 888–896, 2009.
- 431 Derksen, J., Roelofs, G.-J., and Röckmann, T.: Influence of entrainment of CCN on microphysical properties of warm
 432 cumulus, *Atmospheric chemistry and physics*, 9, 6005–6015, 2009.
- 433 Desai, N., Liu, Y., Glienke, S., Shaw, R. A., Lu, C., Wang, J., and Gao, S.: Vertical Variation of Turbulent Entrainment
 434 Mixing Processes in Marine Stratocumulus Clouds Using High - Resolution Digital Holography, *Journal of Geophysical*
 435 *Research: Atmospheres*, 126, e2020JD033527, 2021.
- 436 Freud, E., Rosenfeld, D., Andreae, M., Costa, A., and Artaxo, P.: Robust relations between CCN and the vertical evolution of
 437 cloud drop size distribution in deep convective clouds, *Atmospheric Chemistry and Physics*, 8, 1661–1675, 2008.
- 438 Freud, E., Rosenfeld, D., and Kulkarni, J. R.: Resolving both entrainment-mixing and number of activated CCN in deep
 439 convective clouds, *Atmospheric Chemistry and Physics*, 11, 12887–12900, 10.5194/acp-11-12887-2011, 2011.
- 440 Gao, W., Sui, C. H., Fan, J., Hu, Z., and Zhong, L.: A study of cloud microphysics and precipitation over the Tibetan Plateau
 441 by radar observations and cloud - resolving model simulations, *Journal of Geophysical Research Atmospheres*, 121, 13,735–
 442 713,752, 2016.
- 443 Gao, Z., Liu, Y., Li, X., and Lu, C.: Investigation of turbulent entrainment - mixing processes with a new particle - resolved
 444 direct numerical simulation model, *Journal of Geophysical Research: Atmospheres*, 123, 2194–2214, 2018.
- 445 Gerber, H., Frick, G., Malinowski, S. P., Kumala, W., and Krueger, S.: POST—A new look at stratocumulus, *American*
 446 *Meteorological Society 13th Conference on Cloud Physics*, 2010.
- 447 Gerber, H., Frick, G., Malinowski, S. P., Jonsson, H., Khelif, D., and Krueger, S. K.: Entrainment rates and microphysics in
 448 POST stratocumulus, *Journal of Geophysical Research: Atmospheres*, 118, 12,094–012,109, 2013.
- 449 Gerber, H., Malinowski, S. P., and Jonsson, H.: Evaporative and radiative cooling in POST stratocumulus, *Journal of the*
 450 *Atmospheric Sciences*, 73, 3877–3884, 2016.
- 451 Gerber, H. E., Frick, G. M., Jensen, J. B., and Hudson, J. G.: Entrainment, mixing, and microphysics in trade-wind cumulus,
 452 *Journal of the Meteorological Society of Japan. Ser. II*, 86, 87–106, 2008.
- 453 Grabowski, W. W.: Indirect impact of atmospheric aerosols in idealized simulations of convective–radiative quasi

454 equilibrium, *Journal of climate*, 19, 4664-4682, 10.1175/JCLI3857.1, 2006.

455 Haman, K. E., Malinowski, S. P., Kurowski, M. J., Gerber, H., and Brenguier, J.-L.: Small scale mixing processes at the top
456 of a marine stratocumulus—a case study, *Quarterly Journal of the Royal Meteorological Society*, 133, 213-226, 10.1002/qj.5,
457 2007.

458 Hill, S. A., Krueger, S., Gerber, H., and Malinowski, S.: Entrainment interface layer of stratocumulus-topped boundary
459 layers during POST, 13 AMS Conf. On Cloud Phys, 2010.

460 Hoffmann, F., and Feingold, G.: Entrainment and Mixing in Stratocumulus: Effects of a New Explicit Subgrid-Scale Scheme
461 for Large-Eddy Simulations with Particle-Based Microphysics, *Journal of the Atmospheric Sciences*, 76, 1955-1973,
462 10.1175/jas-d-18-0318.1, 2019.

463 Hudson, James, G., Yum, Seong, and Soo: Droplet spectral broadening in marine stratus, *Journal of the Atmospheric
464 Sciences*, 1997.

465 Jarecka, D., Grabowski, W. W., Morrison, H., and Pawlowska, H.: Homogeneity of the subgrid-scale turbulent mixing in
466 large-eddy simulation of shallow convection, *Journal of the atmospheric sciences*, 70, 2751-2767, 2013.

467 Jen-La Plante, I., Ma, Y., Nurowska, K., Gerber, H., Khelif, D., Karpinska, K., Kopec, M. K., Kumala, W., and Malinowski,
468 S. P.: Physics of Stratocumulus Top (POST): turbulence characteristics, *Atmospheric Chemistry and Physics*, 16, 9711, 2016.

469 Jensen, J., Austin, P., Baker, M., and Blyth, A.: Turbulent mixing, spectral evolution and dynamics in a warm cumulus cloud,
470 *Journal of the atmospheric sciences*, 42, 173-192, 10.1175/1520-0469(1985)042<0173:TMSEAD>2.0.CO;2, 1985.

471 Jones, C., Bretherton, C., and Leon, D.: Coupled vs. decoupled boundary layers in VOCALS-REx, *Atmospheric Chemistry
472 and Physics*, 11, 7143-7153, 2011.

473 Khain, A., Pinsky, M., and Magaritz - Ronen, L.: Physical interpretation of mixing diagrams, *Journal of Geophysical
474 Research: Atmospheres*, 123, 529-542, 2018.

475 Kumala, W., Haman, K., Kopec, M., Khelif, D., and Malinowski, S.: Modified ultrafast thermometer UFT-M and
476 temperature measurements during Physics of Stratocumulus Top (POST), *Atmospheric Measurement Techniques*, 6, 2043-
477 2054, 2013.

478 Kumar, B., Janetzko, F., Schumacher, J. R., and Shaw, R. A.: Extreme responses of a coupled scalar–particle system during
479 turbulent mixing, *New Journal of Physics*, 14, 115020, 2012.

480 Kumar, B., Schumacher, J., and Shaw, R. A.: Cloud microphysical effects of turbulent mixing and entrainment, *Theoretical
481 and Computational Fluid Dynamics*, 27, 361-376, 10.1007/s00162-012-0272-z, 2013.

482 Kumar, B., Götzfried, P., Suresh, N., Schumacher, J., and Shaw, R. A.: Scale Dependence of Cloud Microphysical Response
483 to Turbulent Entrainment and Mixing, *Journal of Advances in Modeling Earth Systems*, 10, 2777-2785, 2018.

484 Lasher - trapp, S. G., Cooper, W. A., and Blyth, A. M.: Broadening of droplet size distributions from entrainment and mixing
485 in a cumulus cloud, *Quarterly Journal of the Royal Meteorological Society: A journal of the atmospheric sciences, applied
486 meteorology and physical oceanography*, 131, 195-220, 10.1256/qj.03.199, 2005.

487 Lehmann, K., Siebert, H., and Shaw, R. A.: Homogeneous and Inhomogeneous Mixing in Cumulus Clouds: Dependence on
488 Local Turbulence Structure, *Journal of the Atmospheric Sciences*, 66, 3641-3659, 10.1175/2009jas3012.1, 2009.

489 Liu, Y., Daum, P. H., Chai, S. K., and Liu, F.: Cloud parameterizations, cloud physics, and their connections: an overview,
490 Brookhaven National Lab., Upton, NY (US), 2002.

491 Lu, C., Liu, Y., and Niu, S.: Examination of turbulent entrainment - mixing mechanisms using a combined approach, *Journal
492 of Geophysical Research: Atmospheres*, 116, 10.1029/2011JD015944, 2011.

493 Lu, C., Liu, Y., Niu, S., and Vogelmann, A. M.: Lateral entrainment rate in shallow cumuli: Dependence on dry air sources
494 and probability density functions, *Geophysical Research Letters*, 39, 2012.

495 Lu, C., Liu, Y., and Niu, S.: A method for distinguishing and linking turbulent entrainment mixing and collision-coalescence
496 in stratocumulus clouds, *Chin. Sci. Bull.*, 58, 545-551, 2013a.

497 Lu, C., Liu, Y., Niu, S., Krueger, S., and Wagner, T.: Exploring parameterization for turbulent entrainment-mixing processes
498 in clouds, *Journal of Geophysical Research Atmospheres*, 118, 185-194, 2013b.

499 Lu, C., Niu, S., Liu, Y., and Vogelmann, A. M.: Empirical relationship between entrainment rate and microphysics in
500 cumulus clouds, *Geophysical Research Letters*, 40, 2333-2338, 10.1002/grl.50445, 2013c.

501 Lu, C., Liu, Y., and Niu, S.: Entrainment-mixing parameterization in shallow cumuli and effects of secondary mixing events,
502 Science China Press, 2014a.

503 Lu, C., Liu, Y., Niu, S., and Endo, S.: Scale dependence of entrainment-mixing mechanisms in cumulus clouds, *Journal of*
504 *Geophysical Research: Atmospheres*, 119, 13,877-813,890, 10.1002/2014jd022265, 2014b.

505 Lu, C., Liu, Y., Zhu, B., Yum, S. S., Krueger, S. K., Qiu, Y., Niu, S., and Luo, S.: On Which Microphysical Time Scales to
506 Use in Studies of Entrainment - Mixing Mechanisms in Clouds, *Journal of Geophysical Research: Atmospheres*, 123, 3740-
507 3756, 2018.

508 Luo, S., Lu, C., Liu, Y., Bian, J., Gao, W., Li, J., Xu, X., Gao, S., Yang, S., and Guo, X.: Parameterizations of Entrainment -
509 Mixing Mechanisms and Their Effects on Cloud Droplet Spectral Width Based on Numerical Simulations, *Journal of*
510 *Geophysical Research: Atmospheres*, 125, e2020JD032972, 2020.

511 Ma, Y.-F., Malinowski, S. P., Karpińska, K., Gerber, H. E., and Kumala, W.: Scaling analysis of temperature and liquid water
512 content in the marine boundary layer clouds during POST, *Journal of the Atmospheric Sciences*, 74, 4075-4092, 2017.

513 Ma, Y. F., Pedersen, J., Grabowski, W., Kopec, M., and Malinowski, S.: Influences of Subsidence and Free - Tropospheric
514 Conditions on the Nocturnal Growth of Nonclassical Marine Stratocumulus, *Journal of Advances in Modeling Earth Systems*,
515 10, 2706-2730, 2018.

516 Malinowski, S. P., Haman, K., Kumala, W., Kopec, M., Gerber, H., and Krueger, S.: Smallscale variability of temperature
517 and LWC at stratocumulus top, 13 AMS Conf. On Cloud Phys., th, 2010.

518 Malinowski, S. P., Gerber, H., Jen-La Plante, I., Kopec, M. K., Kumala, W., Nurowska, K., Chuang, P. Y., Khelif, D., and
519 Haman, K. E.: Physics of Stratocumulus Top (POST): turbulent mixing across capping inversion, *Atmospheric Chemistry*
520 *and Physics*, 13, 12171-12186, 2013.

521 Meischner, P., Baumann, R., and Holler, H.: Eddy Dissipation Rates in Thunderstorms Estimated by Doppler Radar in
522 Relation to Aircraft In Situ Measurements, *Journal of Atmospheric & Oceanic Technology*, 18, 1609-1627, 2001.

523 Morrison, A. G.: Advanced Two-Moment Bulk Microphysics for Global Models. Part I: Off-Line Tests and Comparison with
524 Other Schemes, *Journal of Climate*, 28, 1288-1307, 2015.

525 Panofsky, H. A.: Atmospheric turbulence, Models and methods for engineering applications., 397, 1984.

526 Pawlowska, H., Brenguier, J., and Burnet, F.: Microphysical properties of stratocumulus clouds, *Atmospheric research*, 55,
527 15-33, 10.1016/S0169-8095(00)00054-5, 2000.

528 Shupe, M., Persson, P., Brooks, I., Tjernström, M., Sedlar, J., Mauritsen, T., Sjogren, S., and Leck, C.: Cloud and boundary
529 layer interactions over the Arctic sea ice in late summer, *Atmospheric Chemistry and Physics*, 13, 9379-9399, 2013.

530 Siebert, H., Franke, H., Lehmann, K., Maser, R., Saw, E. W., Schell, D., Shaw, R. A., and Wendisch, M.: Probing finescale
531 dynamics and microphysics of clouds with helicopter-borne measurements, *Bull. Amer. Meteor. Soc*, 87, 1727-1738, 2006.

532 Small, J. D., Chuang, P. Y., and Jonsson, H. H.: Microphysical imprint of entrainment in warm cumulus, *Tellus B: Chemical*
533 *and Physical Meteorology*, 65, 19922, 2013.

534 Stephens, G. L.: Cloud feedbacks in the climate system: A critical review, *Journal of climate*, 18, 237-273, 10.1175/JCLI-
535 3243.1, 2005.

536 Stevens, B.: Cloud transitions and decoupling in shear - free stratocumulus - topped boundary layers, *Geophysical research*
537 *letters*, 27, 2557-2560, 2000.

538 Su, C.-W., Krueger, S. K., McMurtry, P. A., and Austin, P. H.: Linear eddy modeling of droplet spectral evolution during
539 entrainment and mixing in cumulus clouds, *Atmospheric research*, 47, 41-58, 10.1016/S0169-8095(98)00039-8, 1998.

540 Telford, J.: Clouds with turbulence; the role of entrainment, *Atmospheric research*, 40, 261-282, 10.1016/0169-
541 8095(95)00038-0, 1996.

542 Telford, J. W., and Chai, S. K.: A new aspect of condensation theory, pure and applied geophysics, 118, 720-742,
543 10.1007/bf01593025, 1980.

544 Wang, J., Daum, P. H., Yum, S. S., Liu, Y., Senum, G. I., Lu, M.-L., Seinfeld, J. H., and Jonsson, H.: Observations of marine
545 stratocumulus microphysics and implications for processes controlling droplet spectra: Results from the Marine
546 Stratus/Stratocumulus Experiment, *Journal of Geophysical Research*, 114, 10.1029/2008jd011035, 2009.

547 Wang, Y.: *Aerosol-Cloud Interactions from Urban, Regional, to Global Scales*, Springer, 2015.

548 Wang, Y., Niu, S., Lv, J., Lu, C., Xu, X., Wang, Y., Ding, J., Zhang, H., Wang, T., and Kang, B.: A new method for
549 distinguishing unactivated particles in cloud condensation nuclei (CCN) measurements: Implications for aerosol indirect
550 effect evaluation, *Geophysical Research Letters*, 2019.

551 Wood, R.: Stratocumulus clouds, *Monthly Weather Review*, 140, 2373-2423, 2012.

552 Wyngaard, J. C.: *Turbulence in the Atmosphere*, Cambridge University Press, 2010.

553 Xu, X., and Xue, H.: Impacts of free-tropospheric temperature and humidity on nocturnal nonprecipitating marine
554 stratocumulus, *Journal of the Atmospheric Sciences*, 72, 2853-2864, 2015.

555 Xu, X., Lu, C., Liu, Y., Gao, W., Wang, Y., Cheng, Y., Luo, S., and Weverberg, K. V.: Effects of Cloud Liquid - Phase
556 Microphysical Processes in Mixed - Phase Cumuli Over the Tibetan Plateau, *Journal of Geophysical Research: Atmospheres*,
557 125, 2020.

558 Xue, H., and Feingold, G.: Large-eddy simulations of trade wind cumuli: Investigation of aerosol indirect effects, *Journal of*
559 *the Atmospheric Sciences*, 63, 1605-1622, 10.1175/JAS3706.1, 2006.

560 Yau, M. K., and Rogers, R. R.: *A short course in cloud physics*, Elsevier, 1996.

561 Yeom, J. M., Yum, S. S., Liu, Y., and Lu, C.: A study on the entrainment and mixing process in the continental stratocumulus
562 clouds measured during the RACORO campaign, *Atmospheric Research*, 194, 89-99, 10.1016/j.atmosres.2017.04.028, 2017.

563 Yum, S. S., Wang, J., Liu, Y., Senum, G., Springston, S., McGraw, R., and Yeom, J. M.: Cloud microphysical relationships
564 and their implication on entrainment and mixing mechanism for the stratocumulus clouds measured during the VOCALS
565 project, *Journal of Geophysical Research: Atmospheres*, 120, 5047-5069, 10.1002/2014jd022802, 2015.

566 Zhang, Q., Quan, J., Tie, X., Huang, M., and Ma, X.: Impact of aerosol particles on cloud formation: Aircraft measurements
567 in China, *Atmos. Environ*, 45, 665-672, 2011.

568 Zhao, C., and Garrett, T. J.: Effects of Arctic haze on surface cloud radiative forcing, *Geophysical Research Letters*, 42, 557-
569 564, 2015.

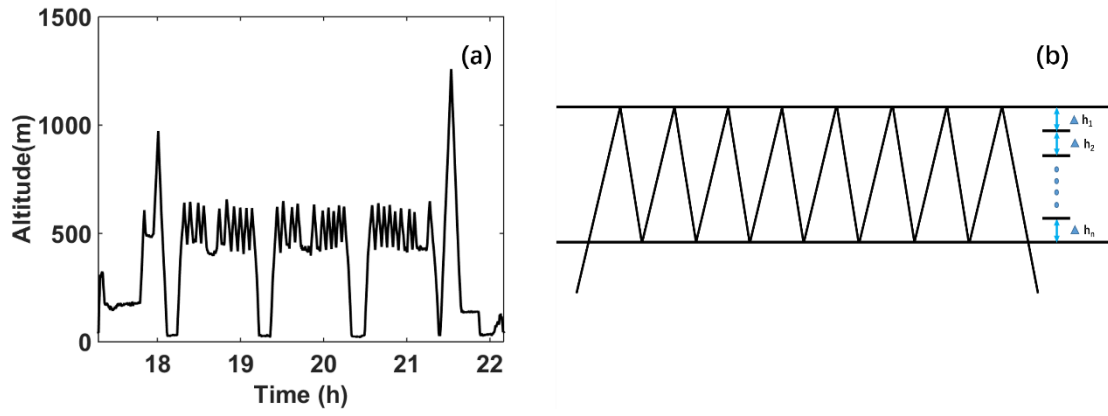
570 Zheng, Y., and Rosenfeld, D.: Linear relation between convective cloud base height and updrafts and application to satellite
571 retrievals, *Geophysical Research Letters*, 42, 6485-6491, 2015.

572 Zheng, Y., Rosenfeld, D., and Li, Z.: Quantifying cloud base updraft speeds of marine stratocumulus from cloud top radiative
573 cooling, *Geophysical Research Letters*, 43, 11,407-411,413, 2016.

574 Zheng, Y., Rosenfeld, D., and Li, Z.: A more general paradigm for understanding the decoupling of stratocumulus - topped
575 boundary layers: The importance of horizontal temperature advection, *Geophysical Research Letters*, 47, e2020GL087697,
576 2020.

577

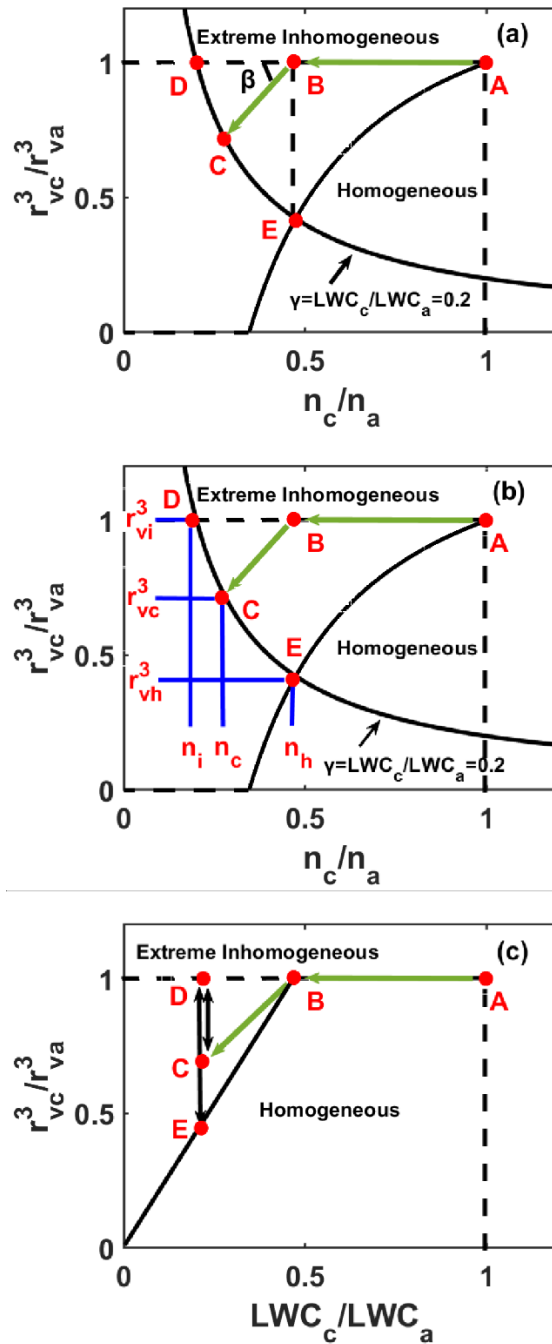
Number	Methods
1	<p>LWC_a: calculated from the adiabatic growth from cloud base; n_a: maximum number concentration in each level; r_{va}: calculated by $r_{va} = \sqrt[3]{\frac{LWC_a}{\frac{4}{3}\pi\rho_L n_a}}$.</p>
2	<p>LWC_a: calculated from the adiabatic growth from cloud base; r_{va}: maximum volume mean radius in each level; n_a: calculated by $n_a = \frac{LWC_a}{\frac{4}{3}\pi\rho r_{va}^3}$.</p>
3	<p>LWC_a: maximum liquid water content in each level n_a: maximum number concentration in each level; r_{va}: calculated by $r_{va} = \sqrt[3]{\frac{LWC_a}{\frac{4}{3}\pi\rho n_a}}$.</p>
4	<p>LWC_a: maximum liquid water content in each level; r_{va}: maximum volume mean radius in each level; n_a: calculated by $n_a = \frac{LWC_a}{\frac{4}{3}\pi\rho r_{va}^3}$.</p>
5	<p>n_a: maximum number concentration in the interval; r_{va}: maximum volume mean radius in the interval; LWC_a: calculated by $LWC_a = \frac{4}{3}\pi\rho r_{va}^3 n_a$.</p>



580

581 **Figure 1.** (a) Flight track on 16 July 2008. (b) Altitude stratification procedure of the sawtooth patterns, with the mean vertical resolution

582 of 5 m such that $\Delta h_1 = \Delta h_2 = \dots = \Delta h_n = 5$ m.



583

584

Figure 2. Microphysical diagram interpreting the definition for different homogeneous mixing degrees ((a) ψ_1 ; (b) ψ_2, ψ_3 ; (c) ψ_4). The

585

Points A and B represent the adiabatic state and the state after entrainment, respectively. If the extreme inhomogeneous mixing process

586

occurs, the cloud state approaches Point D; if the homogeneous mixing process occurs, the cloud state approaches Point E. The actual

587

mixing and evaporation processes are between the two extremes and cloud state approaches Point C. Extreme inhomogeneous mixing

588

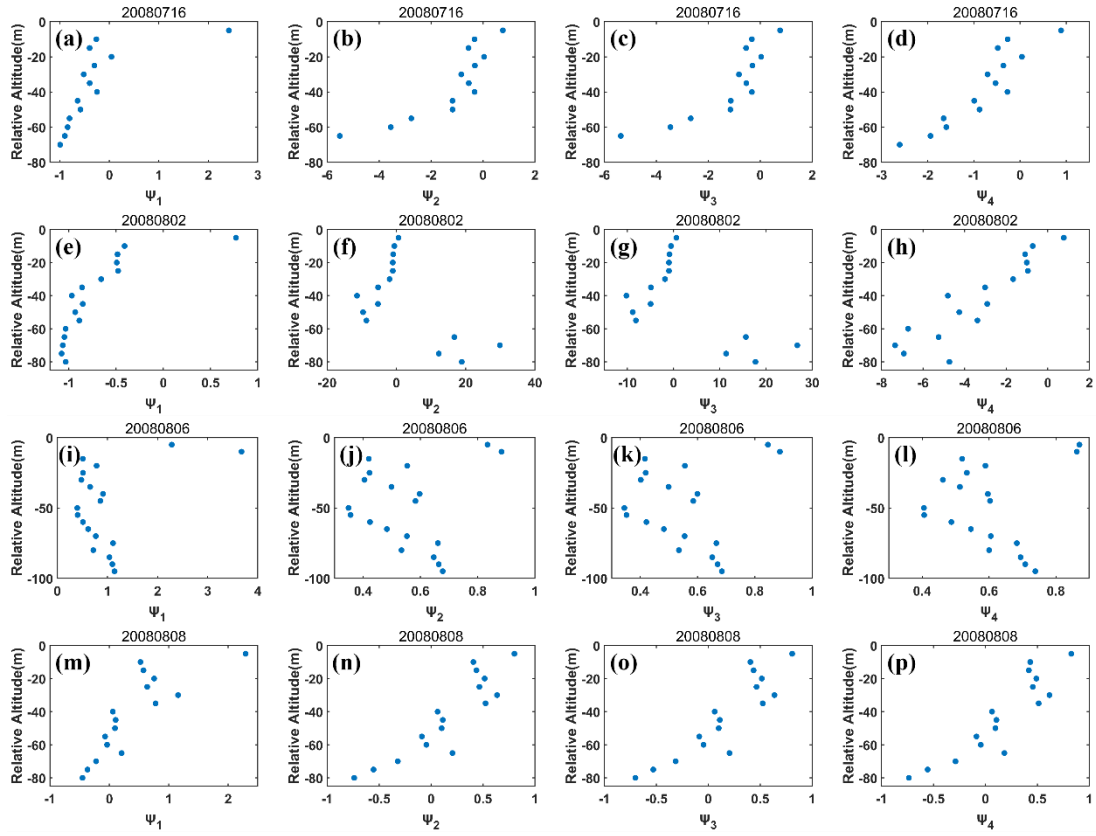
process is represented by the horizontal dashed line; homogeneous mixing process is represented by the solid line starting from Point A in

589

(a) and (b), and the solid line starting from Point B in (c). Another black line in (a) and (b) corresponds to contour of $\gamma = 0.2$ defined as the

590

ratio of liquid water content (LWC_c) to its adiabatic value (LWC_a). See text for the meanings of other symbols.



591

592

593

594

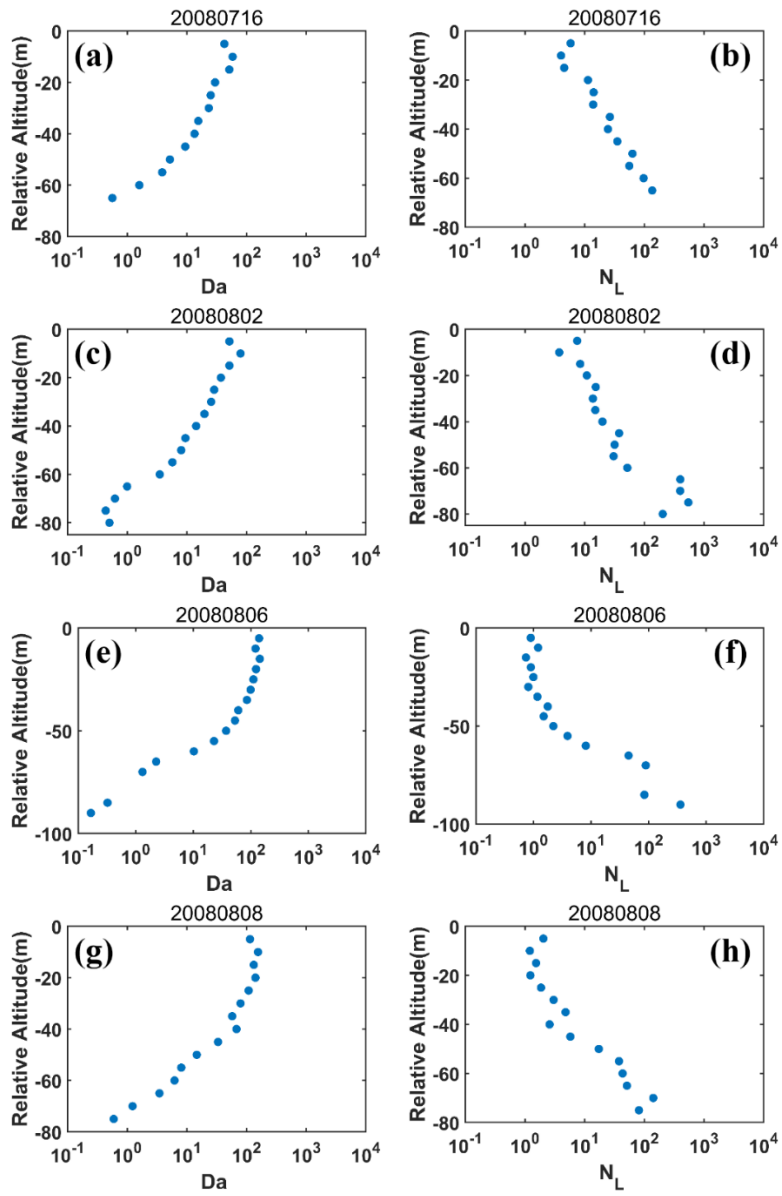
595

596

597

598

Figure 3. Height dependence of the first homogeneous mixing degree (ψ_1) on (a) 16 July 2008, (e) 02 August 2008, (i) 06 August 2008 and (m) 08 August 2008; height dependence of the second homogeneous mixing degree (ψ_2) on (b) 16 July 2008, (f) 02 August 2008, (j) 06 August 2008 and (n) 08 August 2008; height dependence of the third homogeneous mixing degree (ψ_3) on (c) 16 July 2008, (g) 02 August 2008, (k) 06 August 2008 and (o) 08 August 2008; and the fourth homogeneous mixing degree (ψ_4) on (d) 16 July 2008, (h) 02 August 2008, (l) 06 August 2008 and (p) 08 August 2008. The relative altitude on the y-axis equal to 0 represents the cloud tops. Adiabatic liquid water content (LWC_a) is obtained by the adiabatic growth from cloud base, adiabatic number concentration (n_a) is assumed to be the maximum volume mean radius at each level, and adiabatic volume mean radius (r_{va}) is calculated with LWC_a and r_{va} .



599

600

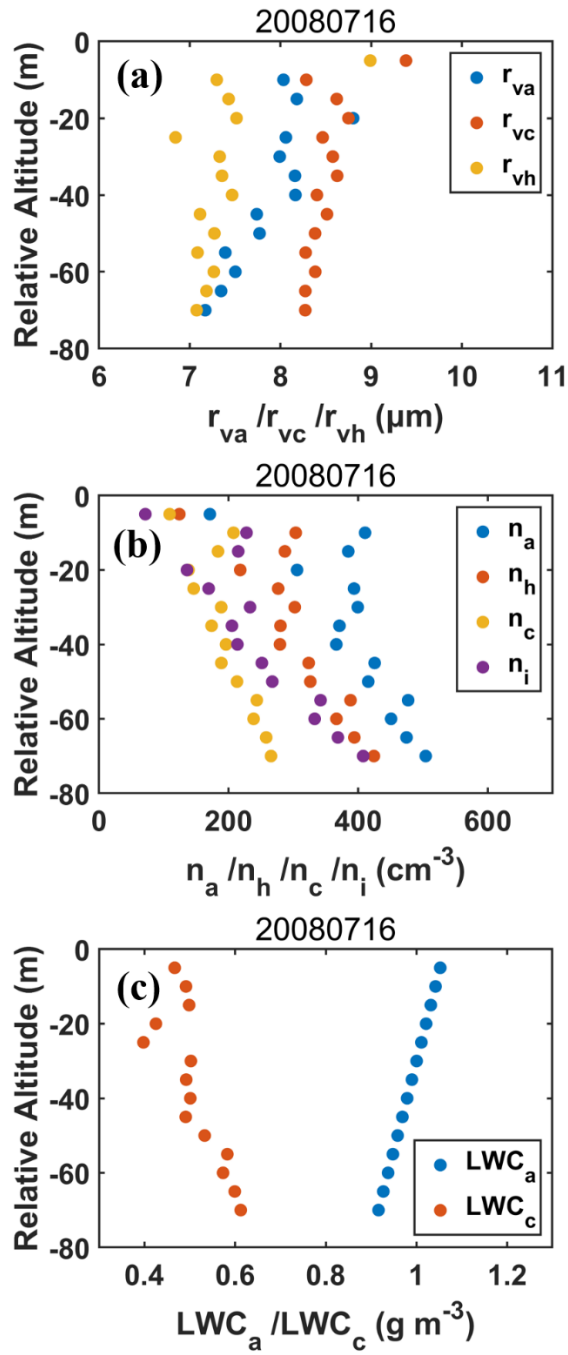
601

602

603

604

Figure 4. Height dependence of Damkohler number (Da) on (a) 16 July 2008, (c) 02 August 2008, (e) 06 August 2008 and (g) 08 August 2008; height dependence of transition scale number (N_L) on (b) 16 July 2008, (d) 02 August 2008, (f) 06 August 2008 and (h) 08 August 2008. The relative altitude on the y-axis equal to 0 represents the cloud tops. Adiabatic liquid water content (LWC_a) is obtained by the adiabatic growth from cloud base, adiabatic number concentration (n_a) is assumed to be the maximum volume mean radius at each level, and adiabatic volume mean radius (r_{va}) is calculated with LWC_a and r_{va} .



605

606

Figure 5. Height dependence of (a) r_{va} , r_{vc} , r_{vh} , (b) n_a , n_h , n_c , n_i and (c) LWC_a , LWC_c on 16 July 2008. The relative altitude on the y-axis

607

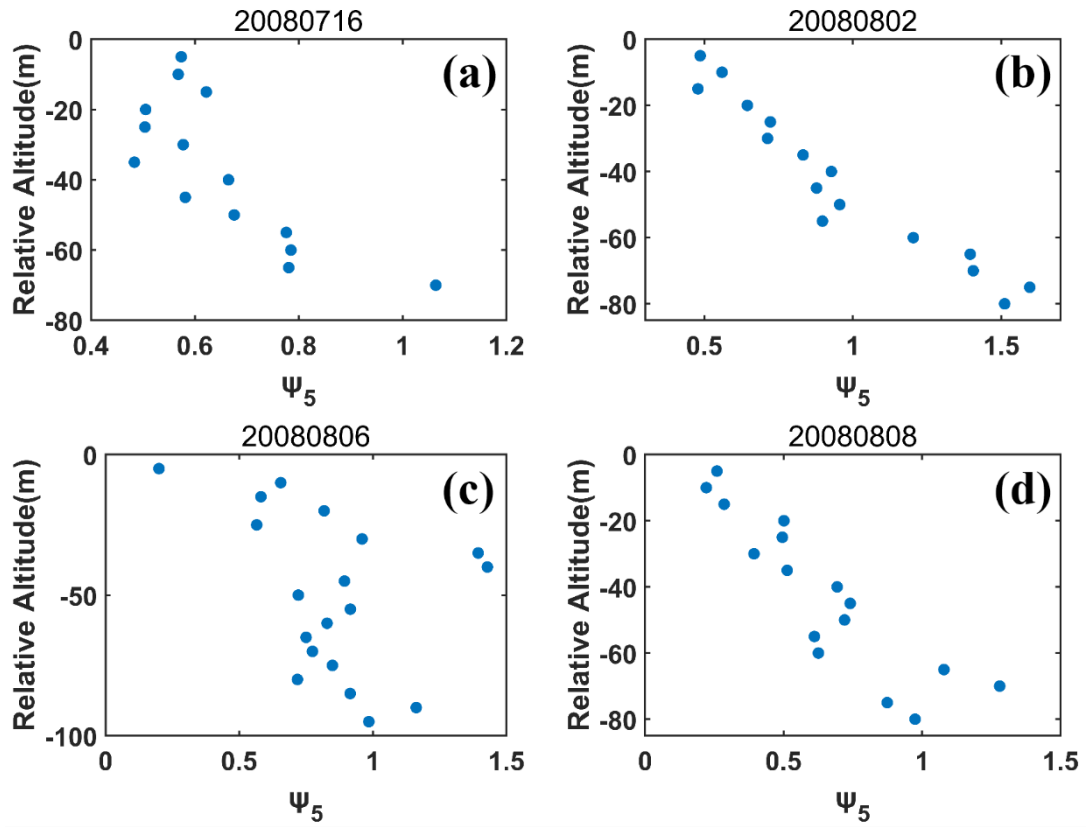
equal to 0 represents the cloud tops. Adiabatic liquid water content (LWC_a) is obtained by the adiabatic growth from cloud base, the

608

maximum number concentration at each level is assumed to be adiabatic number concentration (n_a), and adiabatic volume radius (r_{va}) is

609

calculated with LWC_a and n_a .

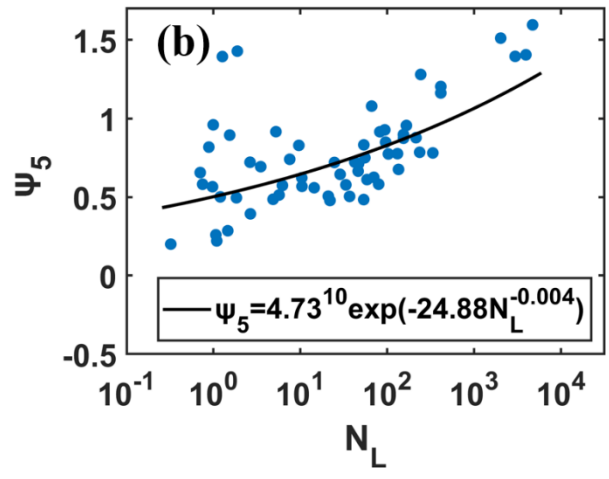
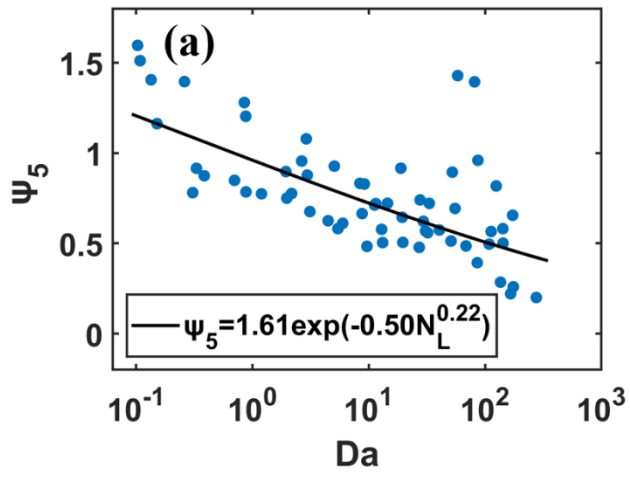


610

611 **Figure 6.** Height dependence of the newly defined homogeneous mixing degree (ψ_5) on (a) 16 July 2008, (b) 02 August 2008, (c) 06

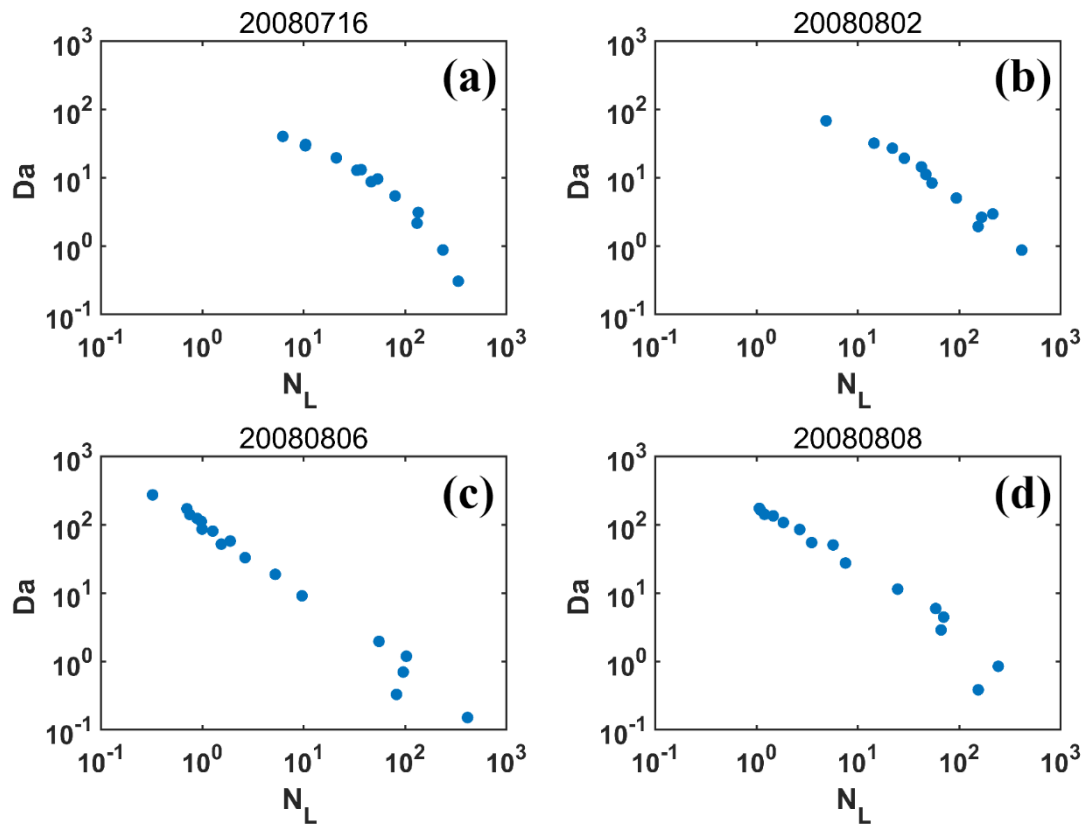
612 August 2008 and (d) 08 August 2008. The relative altitude on the y-axis equal to 0 represents the cloud tops.

613



614

615 **Figure 7.** Relationships of the newly defined homogeneous mixing degree (ψ_5) versus (a) Damkohler number (Da) and (b) transition scale
 616 number (N_L).

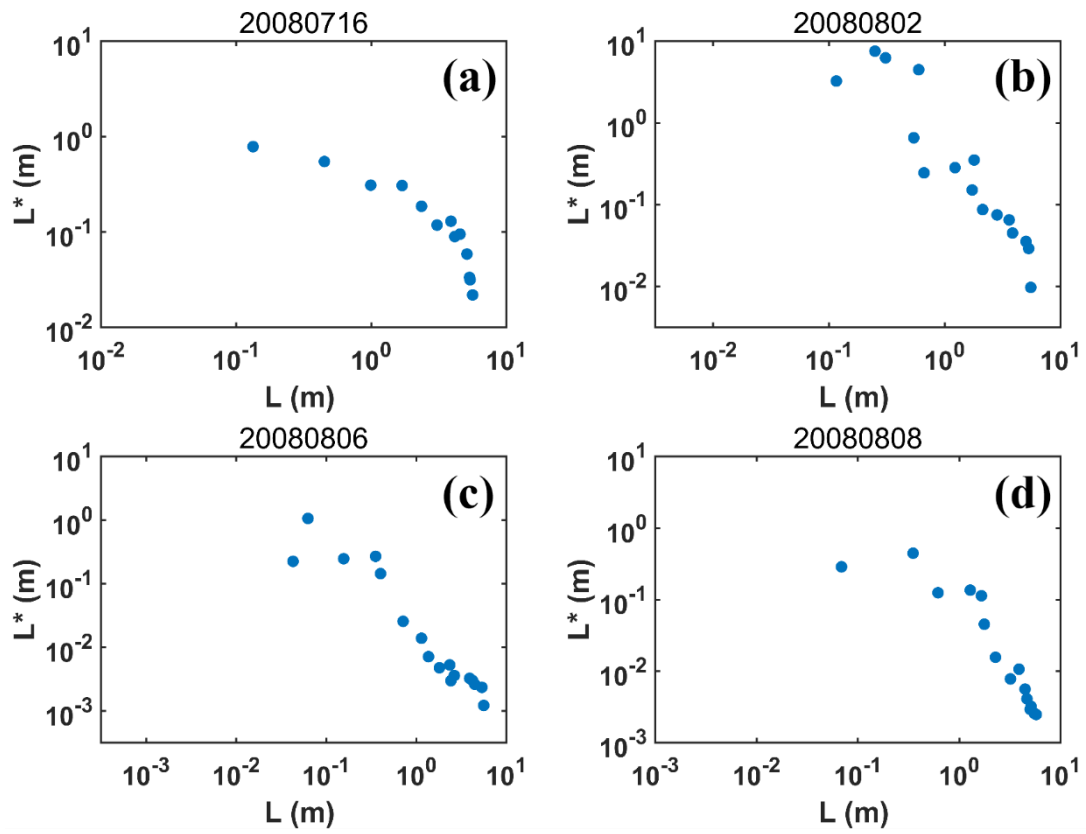


617

618 **Figure 8.** Relationships of Damkohler number (Da) versus transition scale number (N_L) on (a) 16 July 2008, (b) 02 August 2008, (c) 06

619 August 2008 and (d) 08 August 2008.

620

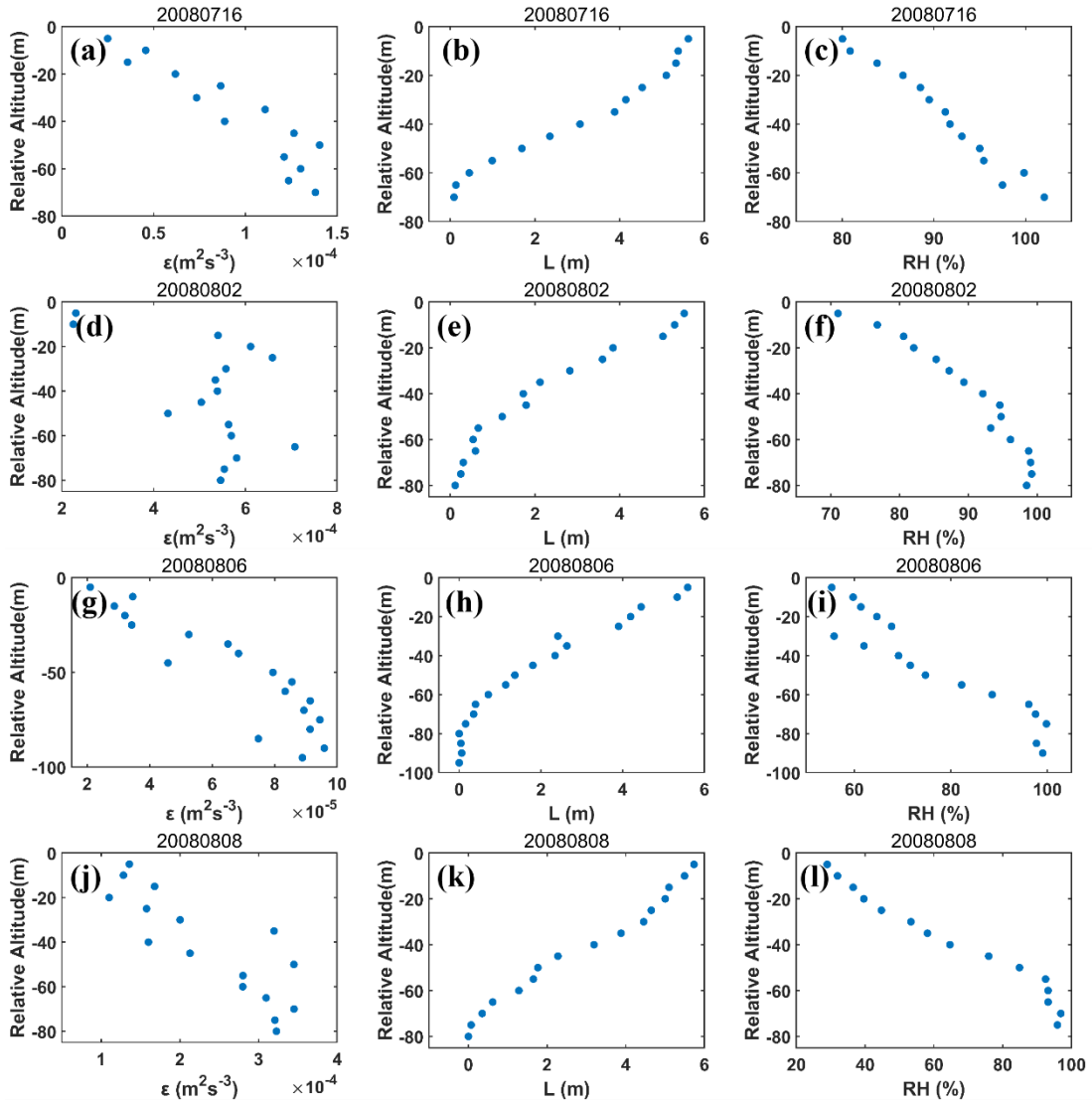


621

622 **Figure 9.** Relationships of transitional scale (L^*) versus droplet-free air length (L) on (a) 16 July 2008, (b) 02 August 2008, (c) 06 August

623 2008 and (d) 08 August 2008.

624



625

626 **Figure 10.** Height dependence of dissipation rate (ϵ) on (a) 16 July 2008, (d) 02 August 2008, (g) 06 August 2008 and (j) 08 August 2008;

627 height dependence of relative humidity (RH) of droplet-free air on (b) 16 July 2008, (e) 02 August 2008, (h) 06 August 2008 and (k) 08

628 August 2008; and height dependence of length of droplet-free air (L) on (c) 16 July 2008, (f) 02 August 2008, (i) 06 August 2008 and (l)

629 08 August 2008. The relative altitude on the y-axis equal to 0 represents the cloud tops.

630